Solid-State ^{93}Nb NMR and ^{93}Nb Nutation Studies of Polycrystalline $Pb(Mg_{1/3}Nb_{2/3})O_3$ and $(1 - x)Pb(Mg_{1/3}Nb_{2/3})O_3/xPbTiO_3$ Solid-Solution Relaxor Ferroelectrics

John J. Fitzgerald,* Subramanian Prasad, Jiong Huang, and Jay S. Shore*

Contribution from the Department of Chemistry and Biochemistry, South Dakota State University, Brookings, South Dakota 57007

Received March 3, 1999. Revised Manuscript Received November 18, 1999

Abstract: Solid-state ^{93}Nb static and MAS NMR and ^{93}Nb nutation studies of polycrystalline $Pb(Mg_{1/3}Nb_{2/3})O_3$, (PMN) and $(1 - x)Pb(Mg_{1/3}Nb_{2/3})O_3/xPbTiO_3$ ($x = 0.05$ to 0.50) solid-solutions are reported. The ^{93}Nb static and MAS NMR spectra of PMN measured at 14.1 T have two major resonances due to the central transition ($^1/_2 \leftrightarrow -^1/_2$), a sharp peak at −902 ppm (1950 Hz fwhh) and a broad resonance (12 800 Hz fwhh) centered at −980 ppm. Two-dimensional ^{93}Nb nutation spectra measured at 9.4 T, by contrast, have three different resonances, a sharp peak due to niobiums with a $C_Q < 0.8$ MHz that is correlated with the sharp ^{93}Nb signal at −902 ppm, and two resonances due to niobiums with a C_Q of ≈ 17 MHz and a $C_Q > 62$ MHz, respectively, that are associated with the broad ^{93}Nb peak centered at −980 ppm. The sharp ^{93}Nb peak for PMN is assigned to Nb(V) B-sites of cubic or high local symmetry in Mg(II)-rich regions with $Nb(OMg)_6$ configurations. The broad ^{93}Nb resonance at −980 ppm is assigned to a range of $Nb(ONb)_{6-x}(OMg)_x$ site configurations, where $x = 0$ to 5, contained in the Nb(V)-rich regions in PMN. The lower symmetry of these Nb(V) B-sites is likely due to neighboring Mg/Nb B-site distributions, that alter the Nb−O bond lengths and O−Nb−O bond angles. Substantially different ^{93}Nb NMR and nutation behavior is observed for $(1 - x)$PMN/xPT powders ($x = 0.05$ to 0.50). Decreased intensity of the sharp −902 ppm peak is due to increasing incorporation of Ti^{4+} ion from PT into the B-sites of $Nb(OMg)_6$ configurations in 5 to 50 mol % PMN/PT solid-solutions. Increasing substitution of Ti^{4+} ions into the Nb(V) B-sites of $Nb(ONb)_{6-x}(OMg)_x$ configurations at higher mol % PT (∼34 to 50 mol % PT) is also correlated with line shape changes of the broad ^{93}Nb NMR peak at −980 ppm and changes in the shape of the contour plots of the nutation spectra. In addition, chemical shift and quadrupolar dispersion effects likely contribute to the observed line shape of the −980 ppm peak for the 0.50PMN/0.50PT sample as a result of B-site occupation by three different cations (Mg^{2+}, Ti^{4+}, and Nb^{5+}) in the different Mg(II)- and Nb(V)-rich substructural regions in PMN/PT materials.

Introduction

The dielectric properties of the class of complex lead perovskite materials with the general formula $Pb(B'_xB''_{1-x})O_3$, where $B' = Zn^{2+}$, Mg^{2+}, Ni^{2+} or Cd^{2+}; $B'' = Nb^{5+}$ or Ta^{5+}, and $PbB'_{1/2}B''_{1/2}O_3$, where $B' = In^{3+}$, $B'' = Nb^{5+}$; and $B' = Sc^{3+}$, $B'' = Nb^{5+}$ or Ta^{5+}, are dependent on both the composition and short- and intermediate-range chemical ordering of the multiple B-sites.[1−7] If the B-sites are randomly occupied by different metal ions, for example, lead zirconate titanates (PZTs), such perovskites exhibit normal ferroelectric or antiferroelectric properties with sharply defined Curie temperatures.[8−11] Perovskites with B-site cation ordering, however, are relaxor ferroelectrics that exhibit broad, diffuse phase transitions and an associated diffuse Curie temperature region.[2,4,5,12−14]

Lead magnesium niobate, $Pb(Mg_{1/3}Nb_{2/3})O_3$, (PMN) is a nonstoichiometric B′B″ lead oxide-based perovskite.[6,7,15−20] PMN undergoes a diffuse phase transition with a maximum temperature, T_M, from −7 to −15 °C.[16] Incorporation of lead titanate (PT) increases T_M by about 5 °C/mol %. Compositions above the morphotropic phase boundary (MPB) (near 34 mol

* To whom correspondence should be addressed.

(1) Lines, M. E.; Glass, A. M. *Principles and Applications of Ferroelectrics and Related Materials*; Clarendon Press: Oxford, 1977.
(2) Jona, F.; Shirane, G. *Ferroelectric Crystals*, Dover: New York, 1993.
(3) Newnham, R. E. Tunable Transducers: Nonlinear Phenomena in Electroceramics. *NIST Spec. Publ.* **1991**, *804*, 39−52.
(4) Cross, L. E. *Ferroelectrics* **1994**, *151*, 305−320.
(5) Shrout, T. R.; Halliyal, A. *Am. Ceram. Soc. Bull.* **1987**, *66*(4), 704−711.
(6) Galasso, F. S. *Structure, Properties and Preparation of Perovskite-Type Compounds;* Pergamon Press: Oxford, 1963; pp 1−121.
(7) Galasso, F.; Pyle, J. *Inorg. Chem.* **1963**, *2*(3), 482−485.
(8) Bursill, L. A.; Peng, J. *NIST Spec. Publ.* **1991**, *804*, 67−76.
(9) Dougherty, T. P.; Wiederrecht, G. P.; Nelson, K. A.; Garrett, M. H.; Jensen, H. P.; Warder, C. *Science* **1992**, *258*, 770−774, and references therein.
(10) (a) Glazer, A. M.; Roleder, K.; Dec, J. *Acta Crystallogr.* **1993**, *B49*, 846−852. (b) Glazer, A. M.; Mabud, S. A. *Acta Crystallogr.* **1978**, *B34*, 1060−1065.
(11) Viehland, D. *Phys. Rev. B* **1995**, *52*, 778−791.
(12) Cross, L. E. *Ferroelectrics* **1987**, *76*, 241−267.
(13) Pan, W. Y.; Gu, W. Y.; Taylor, D. J.; Cross, L. E. *Jpn. J. Appl. Phys.* **1987**, *28*(4), 653−658.
(14) Uchino, K. *Am. Ceram. Soc. Bull.* **1986**, *65*(4), 647−652.
(15) Zhang, Q.; Pan, W.; Bhalla, A.; Cross, L. E. *J. Am. Ceram. Soc.* **1989**, *72*(4), 599−604.
(16) Choi, S. W.; Shrout, T. R.; Jang, S. J.; Bhalla, A. S. *Mater. Lett.* **1989**, *8*(67), 253−255.
(17) Randall, C. A.; Bhalla, A. S.; Shrout, T. R.; Cross, L. E. *J. Mater. Res.* **1990**, *5*(4), 829- 834.
(18) Bursill, L. A.; Qian, H.; Peng, J. L.; Fan, X. D. *Physica B* **1995**, *216*, 1−23.
(19) Ye, Z. G. *Ferroelectrics* **1996**, *184*, 193−208.
(20) Depro, L. E.; Sangaletti, L. *Solid State Commun.* **1997**, *107*, 615−620.

10.1021/ja990688j CCC: $19.00
Published on Web 03/01/2000

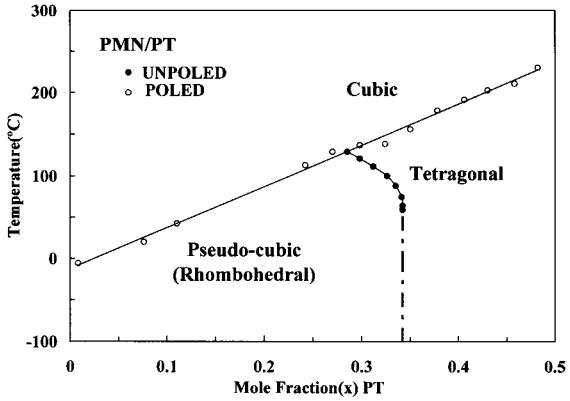

Figure 1. Phase diagram of lead magnesium niobate-lead titanate solid-solution system, $(1-x)Pb(Mg_{1/3}Nb_{2/3})O_3/xPbTiO_3$, (PMN/PT) modified from Choi et al. (refs 16, 67).

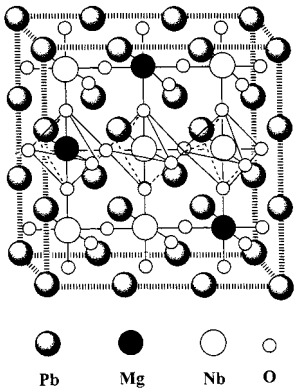

Figure 2. Schematic depiction of perovskite lattice structure of $Pb(Mg_{1/3}Nb_{2/3})O_3$ (PMN) showing the idealized B-site octahedra with 1:2 Mg/Nb ordering.

% PT) undergo pseudo-cubic (*Pm*3*m*) to tetragonal long-range order changes (Figure 1).[16,19] Ceramics with greater than 34 mol % PT are normal ferroelectrics and have a tetragonal lattice structure and dipolar ordering. The PMN-rich solid-solution ceramics near 10 mol % PT are characterized by high dielectric constants and large electrostrictive effects[21−24] that make them ideal for ceramic capacitor, micropositioner, and electrostrictive applications.

The atomic origin of the relaxor ferroelectric behavior of PMN is still not fully understood although there are recent models[4,19,25] based on compositional fluctuations of the B-sites in the perovskite structure. These heterogeneous distributions of Mg/Nb B-site cations lead to the formation of microregions of varying local composition and local phase transition temperatures. Relaxor ferroelectrics have been proposed to exhibit "superparaelectric"[4,19,25,26] behavior due to these small Mg/Nb clusters with short-range order that result in thermally fluctuating dipole moments within a continuously disordered matrix. More recently, a spin glass model[26,27] has been suggested wherein relaxor behavior is a consequence of interactions between the small ordered clusters. PMN ceramics have been shown by high-resolution TEM to exhibit short, coherent long-range order on the nanoscale as a consequence of Mg^{2+}- and Nb^{5+}-rich nanodomain regions.[1,4,13,14,18−20] The B-site cation ordering from 2 to 50 nm,[13,14,18−20,28−34] may be due to short-range ordered regions that are postulated to localize these "superparaelectric" polar clusters,[1,15,19] with the heterogeneous size distributions of these ordered regions accounting for the broad phase transition behavior.

PMN does not exist with an idealized perovskite lattice structure as shown in Figure 2, where an ordered distribution of Mg(II) and Nb(V) ions in the next-nearest neighbor (nnn) B-site octahedra exists; rather, PMN has either partial or complete B-site disorder of the Mg(II) and Nb(V) B-site ions.[18,35−44,48−50] Despite numerous structural studies, there is still a lack of detailed understanding of the atomic-level B-site structure and degree of short-range order in PMN materials that may provide an atomic-level explanation for their relaxor ferroelectric behavior.[19,20] Studies using HRTEM,[18,35] EXAFS,[36] single-crystal X-ray diffraction,[37−41] neutron diffraction,[42] and EPR[43,44] have suggested that there are two B-site nanodomains existing in the three-dimensional structure of PMN, the so-called "1:1 ordered, Mg^{2+}-rich" regions where Mg and Nb ions are arrayed in a successive order (Mg−O−Nb local order) with a 1:1 Mg/Nb mol ratio, and surrounding positively charged "Nb^{5+}-rich" regions (with local Nb−O−Nb ordering) that is required to maintain the charge neutrality.[33,34] Most studies except for recent static ^{93}Nb NMR measurements on single-crystal PMN[45−47]

(21) Norcross, J. A.; Ailion, D. C.; Blinc, R.; Dolinsek, J.; Apih, T.; Slak, J. *Phys. Rev. B* **1994**, *50*(6), 3625−3630.
(22) Yang, M. F.; Ling, H. C.; Rhodes, W. W. *J. Mater. Res.* **1989**, *4*(4), 930−943.
(23) Brown, L. F.; Carlson, R. L.; Sempskott, J. M.; Stranford, G. T.; Fitzgerald, J. J. *Proc. IEEE* **1997**, 561−564.
(24) Swartz, S. L.; Shrout, T. R.; Schulze, W. A.; Cross, L. E. *J. Am. Ceram. Soc.* **1984**, *67*(5), 311−315.
(25) Smolenskii, G. A.; Agronovskaya, A. I. *Sov. Phys. Solid State* **1959**, *1*(10), 1429−1437.
(26) Viehland, D.; Jang, S. J.; Cross, L. E.; Wuttig, M. *J. Appl. Phys.* **1990**, *68*(6), 2916−2921.
(27) Viehland, D.; Jang, S. J.; Cross, L. E.; Wuttig, M. *J. Appl. Phys.* **1990**, *69*(1), 414−419.
(28) Hilton, A. D.; Randall, C. A.; Barber, D. J.; Shrout, T. R. *Ferroelectrics* **1989**, *93*, 379.
(29) Chen, J.; Chan, H. M.; Harmer, M. P. *J. Am. Ceram. Soc.* **1989**, *72*(4), 593−598.
(30) Hilton, A. D.; Barber, D. J.; Randall, C. A.; Shrout, T. R. *J. Mater. Sci.* **1990**, *25*, 3461−3466.
(31) Lin, L. T.; Wu, T. B. *J. Am. Ceram. Soc.* **1990**, *73*, 1253−1256.
(32) Randall, C. A.; Bhalla, A. S. *Jpn. J. Appl. Phys.* **1990**, *29*(2), 327−333.
(33) Newnham, R. E.; Ruschau, G. R. *J. Am. Ceram. Soc.* **1991**, *74*(3), 463.
(34) Newnham, R. E.; Xu, Q. C.; Kumar, S.; Cross, L. E. *Ferroelectrics* **1991**,*102*, 1-B.
(35) de Mathan, N.; Husson, E.; Calvarin, G.; Gavarri, J. R.; Hewat, A. W.; Morell, A. *J. Phys.: Condens. Matter* **1991**, *3*, 8159−8171.
(36) Prouzet, E.; Husson, E.; de Mathan, N.; Morell, A. *J. Phys.: Condens. Matter* **1993**, *5*, 4889−4902.
(37) Zhang, Q. M.; You, H.; Mulvihill, M. L.; Jang, S. F. *Solid State Commun.* **1996**, *97*, 693−698.
(38) Shebonov, L. A.; Kapostins, P. P.; Zvirgzds, *Ferroelectrics* **1984**, *56*, 53−56.
(39) Caranoni, C.; Thuries, F.; Leroux, C.; Nihoul, G. *Philos. Mag. A* **1994**, *69*(3), 633−643.
(40) Bonneau, P.; Garnier, P.; Calvarin, G.; Husson, E.; Gavarri, J. R.; Hewat, A. W.; Morell, A. *J. Solid State Chem.* **1991**, *91*, 350−361.
(41) de Mathan, N.; Husson, E.; Calvarin, G.; Morell, A. *Mater. Res. Bull.* **1991**, *26*, 1167−1172.
(42) Bonneau, P.; Garnier, P.; Husson, E.; Morell, A. *Mater. Res. Bull.* **1989**, *24*, 210−216.
(43) Glinchuk, M. D.; Skorokhod, V.; Bykov, I.; Dimza, V.; Cernovsková, E. *J. Phys. Condens. Mat.* **1994**, *6*, 3421−3428.
(44) Huang, J.; Chasteen, N. D.; Fitzgerald, J. J. *Chem. Mater.* **1998**, *10*(12), 3848−3855.
(45) Glinchuk, M. D.; Bykov, I. P.; Laguta, V. V. *Ferroelectrics* **1991**, *124*, 255−260.
(46) Glinchuk, M. D.; Bykov, I. P.; Laguta, V. V. *Ferroelectrics* **1993**, *143*, 39−47.
(47) Laguta, V. V.; Glinchuk, M. D.; Bykov, I. P.; Van Der Klink, J. J. *Ferroelectrics* **1994**, *156*(4), 2157−2162.
(48) Parmigiani, F.; Rollandi, L.; Samoggia, G.; Depero, L. E. *Solid State Commun.* **1996**, *100*(11), 801−805.
(49) Fitzgerald, J. J.; Huang, J.; Shore, J. S. *Ferroelectrics* **1999**, *233(3−4)*, 187−210.
(50) Prasad, S.; Zhao, P.; Huang, J.; Fitzgerald, J. J.; Shore, J. S. *Solid State Nucl. Magn. Reson.* **1999**, *14*, 231−235.

and XPS results[48] support the 1:1 model.[40,42] XPS results,[48] and recent ^{93}Nb MAS NMR[49] and ^{93}Nb nutation spectroscopy,[50] by contrast, suggest that the B-site ordering is more complex and that Mg^{2+} and Nb^{5+} ions are partially distributed in a random fashion, thus providing charge neutrality by the presence of lead and/or oxygen vacancies. New structural models of PMN based on computer simulations of X-ray reflection data[20,37−40] reveal that PMN has an average cubic structure, with possible intergrowths in the rhombohedral and tetragonal phases.

^{93}Nb is a 100% natural abundant quadrupolar nuclide with a nuclear spin (I) value $I = {}^9/_2$, and a large nuclear quadrupole moment of −0.2 barns. Solid-state ^{93}Nb NMR studies of the ferroelectric alkali metal niobates of lithium, sodium and potassium using principally static, wide-line NMR spectroscopy have been reported.[51−65] Static ^{93}Nb NMR spectra of alkali metal niobates have been used to measure the quadrupolar parameters for lithium niobate ($LiNbO_3$, $C_Q = 22.1$ MHz; $\eta = 0.0$), sodium niobate ($NaNbO_3$, $C_Q = 19.7$ MHz; $\eta = 0.82$) and potasssium niobate ($KNbO_3$, $C_Q = 23.1$ MHz; $\eta = 0.80$).[54−56] The temperature-dependent quadrupolar coupling constant of $NaNbO_3$ varies from 19.7 to 10 MHz as the temperature is increased from room temperature to 270 °C.[58] Wide-line ^{93}Nb NMR spectra of single crystal and nonstoichiometry $LiNbO_3$,[51−54,56] $Ba_2NaNb_5O_{15}$ (BSN),[57] and several magic-angle spinning (MAS) ^{93}Nb NMR spectra (at 9.4 T) for powder and single crystals of $LiNbO_3$, $NaNbO_3$, the layered niobate $KCa_2Nb_3O_{10}$, and $NbVO_5$ have been measured.[59−65] These latter ^{93}Nb MAS NMR spectra have broad resonances for Nb(V) sites due to large residual second-order quadrupolar line-broadening.

In this report, extensive solid-state ^{93}Nb NMR and two-dimensional ^{93}Nb static nutation studies of polycrystalline PMN and a wide range of PMN/PT solid-solution materials are reported. Previous wide-line ^{93}Nb NMR studies of single-crystal PMN[45−47] showed that the ^{93}Nb NMR spectrum is composed of an overlapping fast and a slow-relaxing component, the fast relaxing resonance being attributed to the Nb(V) ion motion in the B-sites. Recently, ^{93}Nb MAS NMR spectra of single-crystal PMN and PZN[49] also showed that these two nonstoichiometric mixed B′B″ perovskites have at least two different types of Nb(V) B-sites, while two-dimensional ^{93}Nb nutation spectra[50] of polycrystalline PMN containing multiple Nb(V) sites shows three different types of ^{93}Nb nutation resonances.

Studies of the local Nb(V) coordination environment in these ferroelectric lead-based niobate perovskites using ^{93}Nb MAS NMR is a formidable challenge that is complicated by limitations of spectral resolution and need for quantitation of isotropic chemical shifts (δ_{iso}) and ^{93}Nb quadrupolar parameters (C_Q and η_Q) to describe the local atomic-level Nb(V) B-site environments. Significant overlap of resonances for several types of Nb(V) sites in PMN[49,50] is the result of incomplete averaging of the second-order quadrupolar contributions of ^{93}Nb resonances, particularly for ^{93}Nb peaks with moderate C_Q (17 to 23 MHz), such as also observed for alkali niobates even at high magnetic field strengths (14.1 T) and fast MAS spinning rates (>15 kHz). For ferroelectric and piezoelectrics perovskites such as PMN and PZN, the distortions in the local pseudo-octahedral NbO_6 sites due to both oxide lattice constraints and different degrees of ordering of the Mg/Nb B-site cations are proposed to cause averaging of the local temperature-dependent motion and/or elastic fluctuations of the crystal lattice, leading to significant line-narrowing of ^{93}Nb resonances.[45−47] Ferroelectric lead-based niobates such as PMN and PZN also have a high degree of local Mg(II)/Nb(V) disorder, due to several different types of Nb(V) sites in nanodomain regions, that result in both chemical shift and quadrupolar dispersion from overlapping ^{93}Nb resonances with different ^{93}Nb chemical shifts or quadrupolar parameters (C_Q and η_Q).[49,50]

The solid-state ^{93}Nb NMR and ^{93}Nb nutation results reported here represent a thorough and detailed investigation of both polycrystalline PMN and a wide range of PMN/PT solid-solutions that clarify the solid-state ^{93}Nb MAS NMR and ^{93}Nb nutation behavior of these systems. These studies are motivated by the need to more fully describe the atomic-level short-range order and local chemical environments of the B-sites Nb(V) ion in PMN and PMN/PT solid-solution systems. Correlations between the ordering in the B-sites (Mg/Nb) and the local chemical environment of different Nb(V) ions in the perovskite lattice, and their known temperature-dependent electrical properties are of primary significance in understanding the materials chemistry of these electronic ceramics. Through the combined use of ^{93}Nb MAS NMR and ^{93}Nb static nutation measurements described here, new and detailed atomic-level information about the Nb(V) B-sites of PMN and related PMN/PT materials throughout the phase diagram region 5 to 50 mol % PT is described. The ^{93}Nb MAS NMR and ^{93}Nb nutation results reported in these investigations demonstrate the complexity and subtleties of the Nb(V) B-site chemical environments in these ferroelectric materials. These studies have advanced our fundamental understanding of the local Nb(V) ion chemical environments, the origin of the short-range chemical Mg/Nb ordering, and the possible motional behavior of the Nb^{5+} (and Mg^{2+}) ions in the B-sites of these relaxor ferroelectrics. These investigations provide conclusive spectroscopic evidence for the existence of at least three different types of Nb(V) ion B-sites with variable ^{93}Nb intensity and line shape for PMN and related PT solid-solutions.

Experimental Section

Reagents and Materials. PbO (Alfa, 99.9995%), Nb_2O_5 (Alfa, 99.9985%), TiO_2 (Anatase, Aldrich, 99.9+%), $PbTiO_3$ (Aldrich, 99+%), and $(MgCO_3)_4Mg(OH)_2{\cdot}H_2O$ (Aldrich, 99%) were used as purchased.

Synthesis of PMN and PMN-PT Powders. Synthesis of PMN by Modified Columbite Method. For the modified columbite method, a 2% excess amount of MgO in the form of $(MgCO_3)_4Mg(OH)_2{\cdot}H_2O$

(51) Peterson, G. E.; Carruthers, J. R. *J. Solid State Chem.* **1969**, *1*, 98−99.
(52) Peterson, G. E.; Carnevale, A. *J. Chem. Phys.* **1972**, *56*(10), 4848−4851.
(53) Peterson, G. E.; Bidenbaugh, P. M. *J. Chem. Phys.* **1968**, *48*, 3402−3406.
(54) Kind. R.; Granicher, H. *Solid State Commun*. **1968**, *6*, 439−440.
(55) Ivanova, E. N.; Yatseako, A. V.; Sergeev, N. A. *Solid State Nucl. Magn. Reson.* **1995**, *4*, 381−385.
(56) Yatsenko. A. V.; Ivanova, E. M. *Phys. Solid State* **1995**, *37*(8), 1237−1240.
(57) Watanabe, Y.; Sota, T.; Suzuki, K.; Iyii, N.; Kitamura, K.; Kimura, S. *J. Phys.: Condens. Matter* **1995**, *7*, 3627−3635.
(58) Wolf, F.; Kline, D.; Story, H. S. *J. Chem. Phys.* **1970**, *53*, 3538−3543.
(59) Meadows, M. D.; Smith, K. A.; Kinsey, R. A.; Rothgeb, M.; Skarjune, R. P.; Oldfield, E. *Proc. Natl. Acad. Sci. U.S.A.* **1982**, *79*, 1351−1355.
(60) Blumel, J.; Born, E.; Metzger, T. *J. Phys. Chem. Solids* **1994**, *55*(71), 589−593.
(61) Gobetto, R.; Harris, R. K.; Apperley, D. C. *J. Magn. Reson*. **1992**, *96*, 119−130.
(62) McDowell, A. F.; Conradi, M. S.; Haase, J. *J. Magn. Reson*. **1996**, *119*, 211−218.
(63) Davis, J.; Tinet, D.; Fripiat, J. J.; Amarillo, J. M.; Casal, B.; Ruiz-Hitzky, E. *J. Mater. Res.* **1991**, *6*(2), 393−400.
(64) Pries de Oliveira, P. G.; Lefebvre, F.; Primet, M.; Eon, J. G.; Volta, J. C. *J. Catal*. **1991**, *130*, 293−305.
(65) Hardin, S.; Hay, D.; Millikan, M.; Sanders, J. V.; Turney, T. W. *Chem. Mater*. **1991**, *3*, 977−998.

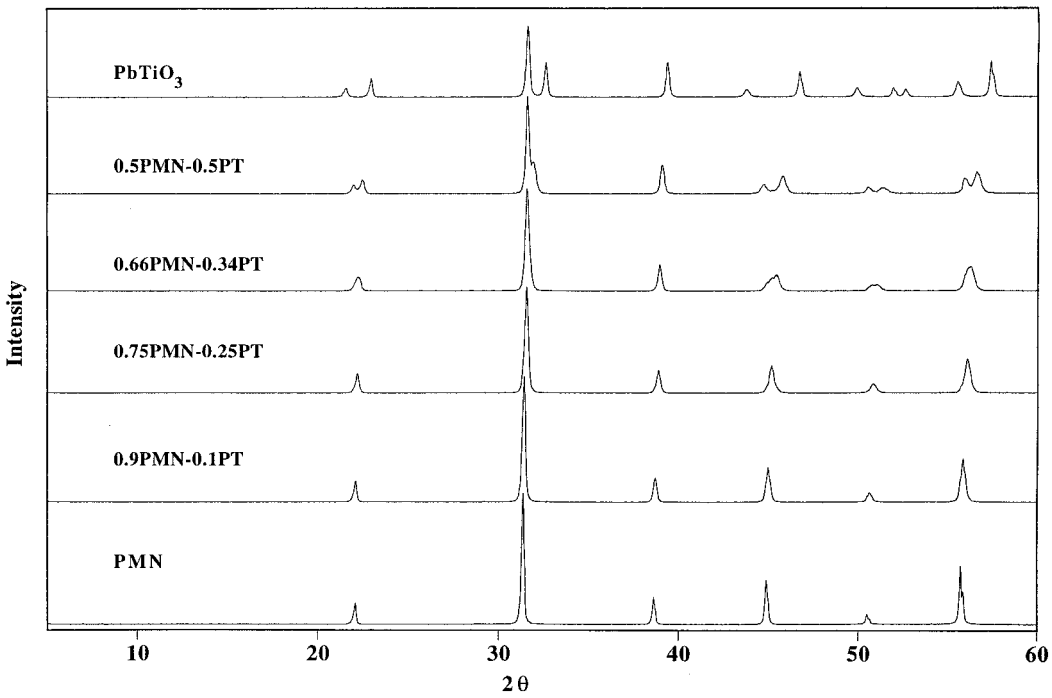

Figure 3. Powder X-ray diffraction patterns of polycrystalline samples of PMN and $(1 - x)$PMN/xPT solid-solutions, where $x = 0.05$ to 0.50 mol % PT.

was used.[44] The $(MgCO_3)_4Mg(OH)_2{\cdot}H_2O$ powder was mixed with Nb_2O_5 powder in an ethanol slurry and ground for 2 h. The resulting paste was dried in an oven (140 °C) overnight and fired at 1000 °C for 6 h. The precursor $MgNb_2O_6$ obtained by this method was mixed with PbO according to the PMN stoichiometry in ethanol for 1.5 h. Following a two-stage calcination as summarized by Gupta and Kulkarni,[66] the dried paste was fired first at 800 °C for 2 h. The resulting light-yellow powder was mixed in an ethanol slurry again for 1 h, the solvent removed by oven drying (140 °C) overnight, and the powder fired at 900 °C for 2 h.

Synthesis of PMN/PT Solid-Solutions.[16,23,24,67] The $(1 - x)$PMN/xPT powders where $x = 0.05$ to 0.50 were prepared using the PMN powder prepared from the modified columbite method. This starting material was mixed with the corresponding mol % PT using Anatase TiO_2 (Aldrich, 99.9+%) and PbO (Alfa, 99.9995%, 0.5% excess). The powder mixture was ground for 1 h in ethanol, dried in an oven (140 °C) overnight and the powder calcined at 900 °C for 4 h.

Chemical Characterization Methods

Powder X-ray Diffraction Analysis. Powder X-ray diffraction analyses were performed using a "Phillips" X-ray diffractometer at the Engineering and Mining Experiment Station, South Dakota School of Mines and Technology, Rapid City, South Dakota. The samples were scanned using Cu Kα at 40 kV and 20 mA. The 2θ scan range was varied from 5 to 60° with scan speeds of 0.02 2θ° per step, at two s per step. The powder XRD patterns for PMN and related PT-solid solution materials studied here are given in Figure 3. XRD and electrical properties measurements of PMN/PT solid solutions have provided the phase diagram for this binary system up to 50 mol % PT as shown in Figure 1.[16] Above 10 mol % PT at room temperature, PMN and PT form a solid-solution with a broad phase transition between the pseudo-cubic (rhombohedral) and cubic lattice structure up to ~34 mol % PT.[35,37−40] The powder XRD diffraction patterns for polycrystalline PMN and PMN/PT samples studied here are consistent with a cubic/pseudo-cubic long-range order for the perovskite lattice structure. For PMN, the XRD diffraction lines are as follows (2θ in deg, *hkl*, relative intensity): 21.88, 100, 14; 31.18, 110, 100; 38.46, 111, 18; 44.73, 200, 31; 50.36, 210, 7; 55.58, 211, 41. The 2θ values of the diffraction lines increase as the amount of PT increases due to the formation of solid-solutions of PMN/PT of a rhombohedral lattice structure. Previous XRD studies[68] determined that this increase in the 2θ values (and corresponding decrease in d spacings) of the XRD lines for PMN/PT materials is due to the changes in the dimensions of the unit cell that are associated with ionic radii differences among the Ti^{4+} (0.61 Å), Nb^{5+} (0.64 Å), and Mg^{2+} (0.72 Å) ions. In addition, for 0.66PMN/0.34PT at the MPB, the increased XRD line widths in comparison with PMN have been interpreted as resulting from overlapping XRD lines due to a mixture of cubic/tetragonal crystal latttice symmetry forms. It should be noted that the splitting of the 2θ reflections at 44.58° and 50.36° in the XRD profile of PMN (Figure 3) is a classic example of the K_α doublet from the $K_{\alpha1}/K_{\alpha2}$ X-ray radiation source, as confirmed by JADE 3.1 (MDI) software.

Solid-State ^{93}Nb NMR Measurements. Solid-state ^{93}Nb static and MAS NMR spectra were measured at 14.1 T (146.8 MHz for ^{93}Nb) using a 16.7 kHz sample spinning rate and a Chemagnetics CMX-600 NMR spectrometer equipped with a "home-built" 3.2 mm sample spinning system and using a Bruker ASX-400 NMR spectrometer at 9.45 T (97.8 MHz for ^{93}Nb) equipped with a "home-built" static probe and a 12.0 mm coil. Single-pulse ^{93}Nb MAS NMR spectra were typically measured using 0.25 μs pulse lengths, 0.200 s delay times, 1.0 μs acquisition delays, with 1000 kHz spectral width (1.0 μs dwell). Spectra were Fourier transformed after two left shifts, seven back-projection points, and exponential line-broadening of 200 Hz were applied. All ^{93}Nb NMR spectra were referenced to an external standard of $NbCl_5$ in "wet" acetonitrile, with the sharp resonance (fwhh = 95 Hz) being assigned a chemical shift of 0.00 ppm.

Two-Dimensional ^{93}Nb Nutation Measurements. All the static ^{93}Nb nutation spectra were measured on a Bruker ASX-400 spectrometer using a "home-built" NMR probe; the samples were packed in glass tubes (12 mm diameter) and mounted perpendicular to the magnetic field. A standard 2D pulse sequence was used for the traditional nutation experiments.[69,70] To obtain pure phase nutation spectra, whole-echo acquisition was used.[50] An original one-pulse nutation experiment was

(66) Gupta, S. M.; Kulkarni, A. R. *Mater. Chem. Phys.* **1994**, *39*, 98−109.

(67) Choi, S. W.; Shrout, T. R.; Jang, S. J.; Bhalla, A. S. *Ferroelectrics* **1989**, *100*, 29−38.

(68) Bouquin, O.; Lejeune, M.; Boilot, J. P. *J. Am. Ceram. Soc.* **1991**, *74*(5), 1152−1156.

(69) (a) Samoson A.; Lippmaa, E. *Phys. Rev. B* **1983**, *28*, 6567−6570. (b) Samoson, A.; Lippmaa, E. *J. Magn. Reson.* **1988**, *79*, 255−268.

(70) Kentgens, A. P. M.; Lemmens, J. J. M.; Gieurtz, F. M. M.; Veeman, W. S. *J. Magn. Reson.* **1989**, *71*, 62−74.

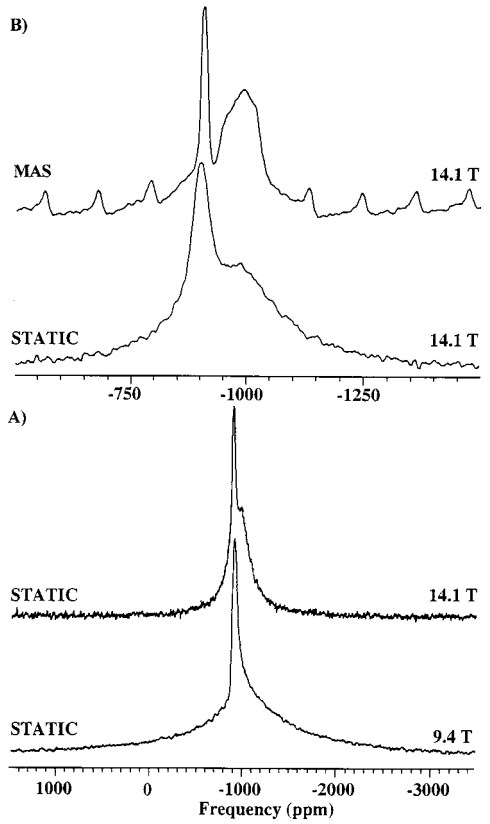

Figure 4. Solid-state ^{93}Nb NMR spectra measured at 9.45 and 14.1 T of polycrystalline samples of PMN: (A) Static spectra with 200 Hz line-broadening showing a sharp and a broader signal. Spectrum at 97.8 MHz was acquired using a Hahn-echo pulse sequence. (B) Static and MAS spectra (at 16.7 kHz sample spinning) of polycrystalline PMN. Experimental conditions: 0.25 μs pulse lengths, 0.200 s delay times, 1.0 μs acquisition delays, with a 1000 kHz spectral width (1.0 μs dwell) and 200 Hz exponential line-broadening.

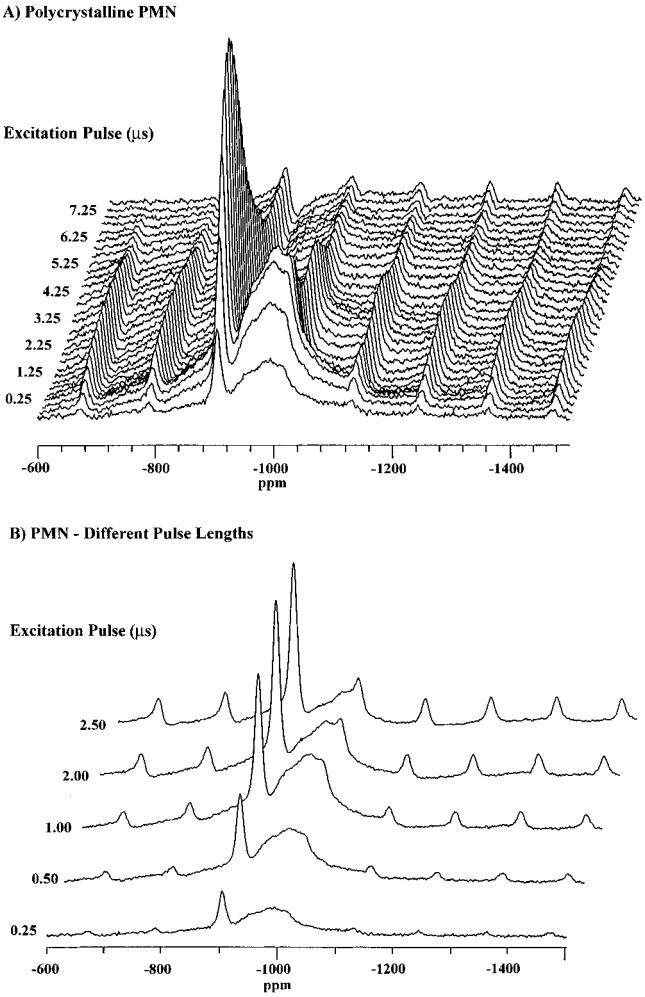

Figure 5. (A) Solid-state ^{93}Nb MAS NMR spectra of polycrystalline PMN powder measured at various excitation pulses from 0.25 to 6.00 μs in 0.25 μs increments, under similar experimental conditions as noted in Figure 4B, and (B) selected ^{93}Nb MAS NMR spectra for PMN powders measured at different pulse lengths.

performed with low rf power (at $\nu_Q \gg \nu_{rf}$); the peak positions in the F1 dimension of the resulting spectrum were used to calculate the length of the π pulse. A small bulb containing the reference solution was placed in the middle of the packed sample tube to account for differences in magnetic susceptibilities of the solid and solution samples. The peak position of the reference solution in the F1 dimension served as an internal reference to accurately measure the 32.5 kHz rf-field used. Typically, 150 t_1 points (512 scans with 100 ms delay) were acquired with 1.0 μs increments. A baseline correction in the F1 dimension was also done.

Results of ^{93}Nb MAS NMR and ^{93}Nb Nutation Studies

Static ^{93}Nb NMR Spectra of PMN at Different Magnetic Field Strengths. The static one-dimensional ^{93}Nb NMR spectra of PMN measured at 9.4 and 14.1 T are shown in Figure 4A. Both spectra have a sharp resonance (fwhh ~8.3 and 9.0 kHz) at −900 ppm and a very broad feature (~200 kHz broad at the baseline at 9.4 T); there is little change in the peak position of the sharp component, implying a small quadrupolar interaction and, hence, a highly symmetric environment for these niobiums. For NMR spectra of quadrupolar nuclei such as ^{93}Nb, severe line-broadening is often observed due to the large quadrupolar interaction. Only the central transition ($+^1/_2 \leftrightarrow -^1/_2$) is normally observed.[49,59−65,71] The central transition may be broadened by dipolar, chemical shift, or second-order quadrupolar effects. The second-order frequency shift of the central transition resonance $\delta_{iso}^{(2Q)}$ is given by the following equation:[72]

$$\delta_{iso}^{(2Q)} = -\frac{3[I(I+1)-3/4]}{40\nu_L^2 I^2(2I-1)^2} C_Q^2\left(1+\frac{\eta_Q^2}{3}\right) \times 10^6 \quad (1)$$

where ν_L is the Larmor frequency, and $C_Q = e^2qQ/h$. Since the line width of the central transition due to the second-order quadrupolar interaction is inversely proportional to the magnetic field strength, and the quadrupolar-induced frequency shift $\delta_{iso}^{(2Q)}$ is inversely proportional to the square of the magnetic field, the narrow and broad components in the ^{93}Nb spectrum measured at 14.1 T are more separated than at 9.4 T. The dominant frequency shift is due to second-order quadrupolar effects. For resonances with a large second-order quadrupolar line-broadening as observed for ^{93}Nb, high resolution is not achieved even at 14.1 T.

Static and MAS ^{93}Nb NMR Spectra of Polycrystalline PMN at 14.1 T. Both static and MAS ^{93}Nb NMR spectra of PMN measured at 14.1 T are shown in Figure 4B. The solid-state ^{93}Nb MAS NMR spectrum of PMN has two major

(71) Man, P. P.; Theveneau, H,; Papon, P. *J. Magn. Reson.* **1985**, *64*, 271−277.

(72) Mueller, K. T.; Baltisberger, J. H.; Wooten, E. W.; Pines, A. *J. Phys. Chem.* **1992**, *96*, 7001−7004.

Table 1. ^{93}Nb MAS NMR Frequency Shifts of PMN, Related PT-Solid Solutions, Alkali Niobates and Lead Niobates (14.1 T)

		^{93}Nb Frequency Shift (ppm) (FWHH, Hz)[c]			^{93}Nb Isotropic Chemical Shift* δ_{iso} (ppm)		
$Pb(Mg_{1/3}Nb_{2/3})O_3$ (PMN), NON-STOICHIOMETRIC PEROVSKITE							
PMN (Crystal)[d]		-902 (2200)	-954 (13400)	-980	-1009[b]		
PMN (Mod. Columbite)		-902 (1950)	-960 (12800)	-980	-1005[b]		
0.90 PMN/0.10 PT (Mod. Columbite)		-906 (2500)	-960 (12800)	-990	-1005[b]		
0.66 PMN/0.34 PT (Mod. Columbite)		-904	(11200)	-995			
0.50 PMN/0.50 PT (Mod. Columbite)			(10000)	-1000			
ALKALI NIOBATE PEROVSKITES							
$LiNbO_3$					-1028 (9800)		(-1000)[a]
$NaNbO_3$					-1102 (6600)		(-1070)[a]
$KNbO_3$					-1069 (10700)		(-1050)[a]
LEAD NIOBATE PYROCHLORES							
$PbNb_2O_6$	(Pb/Nb = 0.50)				-1134 (5000)		(-1115)[a]
$Pb_3Nb_4O_{13}$ (cubic)	(Pb/Nb = 0.75)				-1011 (6000)		(-1000)[a]
$Pb_2Nb_2O_7$	(Pb/Nb = 1.00)		-960(I)[e]		-1014 (5200)		(-1005)[a]
PMN(Py) $Pb_{1.83}Nb_{1.71}Mg_{0.29}O_{6.39}$	(Pb/Nb = 1.06)				-1012 (5800)		(-1000)[a]
$Pb_3Nb_4O_{15}$	(Pb/Nb = 1.25)		-950(I)[e]	-982 (7600)	-1020	(-975)[a]	(-1013)[a]
$Pb_3Nb_2O_8$	(Pb/Nb = 1.50)		-960(I)[e]	-975 (8200)	-1007	(-951)[a]	(-999)[a]

[a] Isotropic chemical shifts derived from simulation of ^{93}Nb MAS spectra measured at various magnetic fields and/or MQMAS results. [b] Significant intensity is from spinning sidebands (ssb) associated with −900 ppm resonance. [c] The numbers in parentheses indicate peak full-widths at half-height in Hertz. [d] Reference 49. [e] (I) Indicates unknown impurity.

resonances, a sharp peak at −902 ppm, and a broad resonance spanning −800 to −1150 ppm. The sharp ^{93}Nb resonance at −902 ppm for PMN is considerably narrowed (11 700 Hz; fwhh = 1950 Hz) using MAS. The broad spectral component spans nearly 350 ppm (51 000 Hz; fwhh = 12 800 Hz) and has three discernible shoulders at −960, −980 and −1000 ppm, the latter being due to a spinning sideband from the −902 ppm signal (vide infra). This broad resonance is likely due to at least two overlapping, incompletely averaged second-order quadrupolar powder patterns (vide infra), each with large quadrupolar coupling constants.

In addition, the ^{93}Nb MAS NMR spectrum shown in Figure 4B has an extensive envelope of spinning sidebands spanning over nearly 4000 ppm (not shown) due to first-order quadrupolar line-broadening contributions of the satellite transitions that are not completely averaged with MAS. The highly symmetrical nature and frequency positions of the spinning sidebands indicate that they are associated with the sharp ^{93}Nb resonance near −902 ppm observed for PMN, whereas spinning sidebands of the broad resonance are not observed due to large quadrupolar interactions. The frequency shift range from −900 to −1200 ppm corresponds to six-coordinate NbO_6 sites (vide infra) as demonstrated from single-pulse ^{93}Nb MAS NMR results and summarized in Table 1 for the alkali metal niobates and various lead niobates.[73,74]

A two-dimensional plot of the ^{93}Nb MAS NMR spectra of PMN as a function of pulse width from 0.2 μs to 7.45 μs is shown in Figure 5A. There are significant changes in the relative intensity of the sharp and broad resonances with increasing excitation pulse width. The intensity of the sharp resonance oscillates with a maximum signal intensity observed at a pulse width of 1.95 μs. The broader resonance reaches a maximum signal intensity between 1.25 and 1.45 μs before decreasing to a null at ∼3.0 μs pulse width. Several of the ^{93}Nb MAS NMR spectra obtained at various pulse widths are shown in Figure 5B. The spectra obtained using 0.25 and 1.50 μs pulses have both the broad and narrow resonances, with the broader resonance decreasing in intensity until it virtually disappears at longer pulse widths (3.0 μs, not shown). The spectrum at 2.5 μs shows that the majority of the spectral intensity for the shoulder component near −1000 ppm (at shorter pulse lengths) is due to spinning sideband intensity associated with the −902

(73) Shore, J. S.; Fitzgerald, J. J., unpublished results 1999.
(74) Fitzgerald, J. J.; Shore, J. S., unpublished results 1999.

ppm peak. Differences in the nutation behavior of the sharp and broad component for PMN indicate that the C_Q of the sharper component is quite small, while the C_Q for the broad resonance is substantial. By Fourier transforming a two-dimensional spectrum similar to Figure 5A, along the excitation pulse dimension, a nutation spectrum is obtained.

Two-dimensional ^{93}Nb Nutation Spectra of PMN. Two-dimensional nutation spectroscopy as introduced by Samoson and Lippmaa[69] has been used to determine quadrupolar coupling constants since the nutation dimension is not affected by the chemical shift interaction.[69,70] In a nutation experiment, the spins precess (nutate) around the $\mathbf{B_1}$ field in the rotating frame at a nutation frequency. For spins with $I = {}^1/_2$, the nutation frequency is $\nu_{rf} = \gamma\mathbf{B_1}$, where γ is the gyromagnetic ratio. For half-integer spins ($I = {}^n/_2$, where $n = 3$, 5, 7, and 9), the situation is complicated. When the quadrupolar interaction is small, the nutation frequency is similar to that of spin $I = {}^1/_2$ nuclei, i.e., $\nu_{rf} = \gamma\mathbf{B_1}$, and for large quadrupolar interactions, the frequency is given by $(I + {}^1/_2)\nu_{rf}$. Recently, a method to measure pure-phase nutation spectra using whole-echo acquisition was reported.[50] This technique avoids problems associated with pulse breakthough and yields higher resolution in both dimensions.

The 2D nutation spectra of PMN obtained with a ν_{rf} of 32.5 kHz and refocusing pulse lengths of 3.4 and 5.6 μs are shown in Figure 6A and 6A′. For the nutation spectra of PMN, a projection of the (F2) axis (not shown) is nearly identical to a static one-dimensional spectrum, while in the nutation (F1) dimension, several distinct features can be identified. The nutation spectrum of PMN measured with a refocusing pulse of 3.4 μs (Figure 6A) has a sharp resonance at $1\nu_{rf}$, and two resonances (a sharp and a broad one) near $5\nu_{rf}$. For the peak at $1\nu_{rf}$, $\nu_Q \ll \nu_{rf}$, and a ν_Q < 32.5 kHz (C_Q of <0.8 MHz) is estimated. It is apparent that a sharp and a very broad component overlap near $5\nu_{rf}$. The broad component is dominant in the nutation dimension with a peak maximum at $5\nu_{rf}$, and with a center of gravity at $\sim 4.5\nu_{rf}$. The overlapping components have been separated by varying the refocusing pulse lengths as shown in Figure 6A and 6A′. The efficiency of the refocusing pulse length depends on the size of the quadrupolar coupling constants of the ^{93}Nb resonances present. In the ^{93}Nb spectrum acquired using a longer refocusing pulse length of 5.6 μs. (Figure 6A′), the narrower of the two components near $5\nu_{rf}$, is predominant. In the nutation dimension, the two resonances at $3.7\nu_{rf}$, and $\sim 1.5\nu_{rf}$, in addition to the peak at $1\nu_{rf}$, are observed. The center of gravity of the sharp and broad resonances near $5\nu_{rf}$ were compared with the theoretical results of Samoson and Lippmaa,[69b] to determine a ν_Q of 700 kHz ($C_Q \approx 17$ MHz) for the sharp component, and a lower limit of 2.6 MHz (C_Q > 62 MHz) for the broad component. Different ^{93}Nb nutation spectra using a range of refocusing pulses have been measured here. A refocusing pulse of 3.4 μs was found optimal for observing all three ^{93}Nb resonances of PMN. A refocusing pulse of 5.6 μs was found optimal for selectively observing the sharp ^{93}Nb resonance with $C_Q \approx 17$ MHz.

Glinchuk et al.[45−47] attributed the changes observed in the temperature-dependent ^{93}Nb NMR spectral line width to motion of the Nb(V) ions in the B-sites of PMN. The observation of two different resonances of sizable C_Q from the ^{93}Nb nutation spectra here indicates significant motion of Nb(V) ions in the B-site environments consistent with this result. Without appreciable motion, the broadest resonance (C_Q > 62 MHz) would be too broad to measure. The presence of three resonances with small, intermediate, and large quadrupolar coupling constants are consistent with one highly symmetrical NbO_6 environment and two types of moderate and highly unsymmetric Nb(V) ion environments in PMN, respectively. The spin-lattice relaxation times (T_1) of 0.6 ms and 10.0 ms for PMN and 0.75PMN/0.25PT,[74] respectively, indicates that rapid thermally induced motion of the Nb(V) ions (and neighboring oxygens) occurs at room temperature that also likely averages the local oxygen

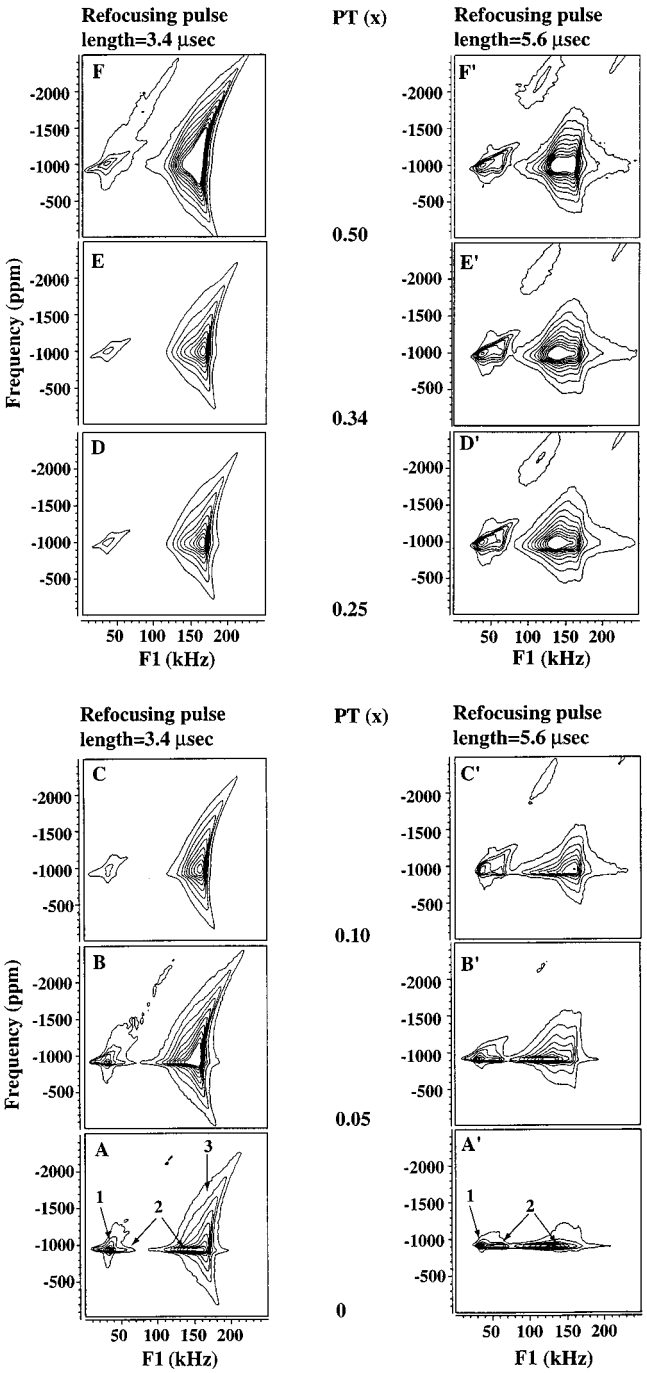

Figure 6. Contour plots of the ^{93}Nb nutation spectra of polycrystalline PMN and $(1 - x)$PMN/xPT powders, where $x = 0.05$, 0.10, 0.25, 0.34, and 0.50 measured using whole-echo acquisition pulse sequence at a refocusing pulse lengths of 3.4 μsec (A−F) and 5.6 μs (A′−F′). Contour levels are drawn from 10 to 100% in 10% increments. The refocusing pulse is set to excite only the central transition. The nutation dimension is plotted along the horizontal axis. The spectra were acquired with a ν_{rf} of 32.5 kHz using the following: 512 transients were acquired for each of the 150 t_1 periods; a 200 μs delay was used between the nutation and the refocusing pulse. A 2 kHz Gaussian and 2 kHz exponential line-broadening were applied in the t_2 and t_1 dimensions, respectively.

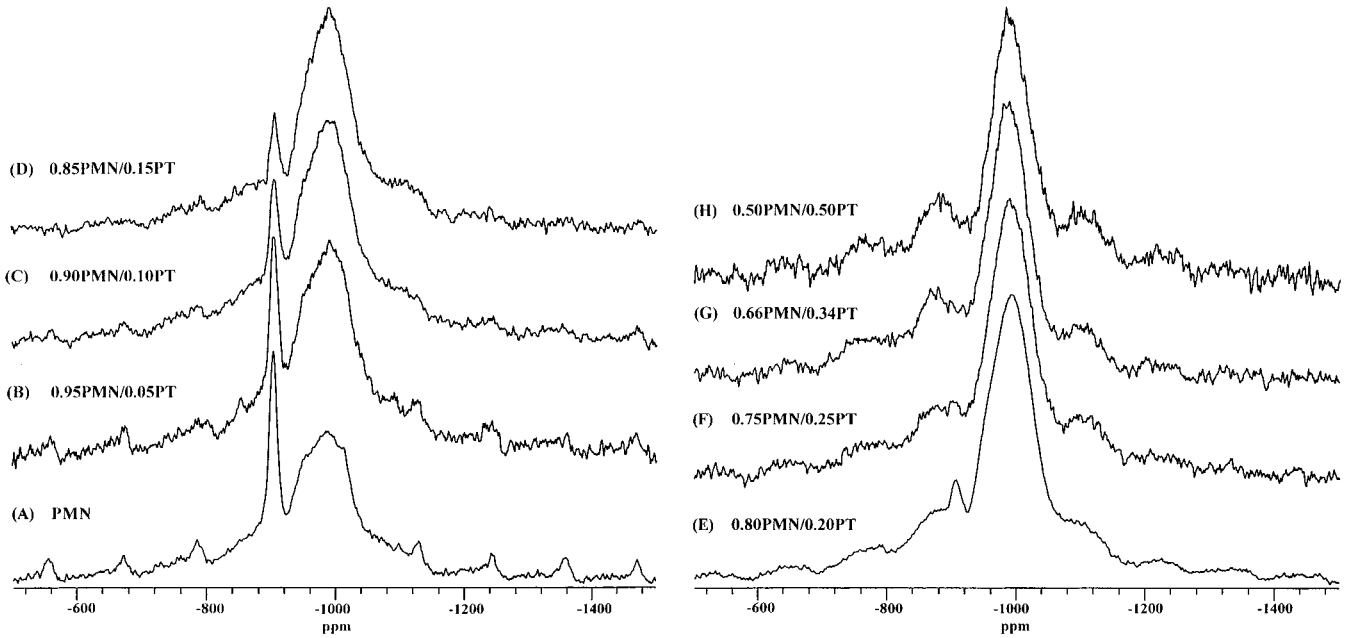

Figure 7. Solid-state ^{93}Nb MAS NMR spectra at 14.1 T of polycrystalline samples of $(1 - x)$PMN/xPT, where $x = 0.00$ to 0.50, over the PMN/PT binary solid-solution phase diagram. Similar experimental conditions as noted in Figure 4B.

chemical environments around the quadrupolar ^{93}Nb nuclei associated with these lower symmetry sites. Such line narrowing due to Nb(V) ion motion at room temperature for PMN (and PMN/PTs) is consistent with the reported thermal-induced motional averaging of Nb(V) B-site ions in single-crystal PMN.[45−47] Detailed studies of the temperature-dependent relaxation behavior and ^{93}Nb NMR spectra of PMN and PMN/PT materials are in progress.

^{93}Nb MAS NMR and ^{93}Nb Nutation Spectra of Polycrystalline PMN/PT Materials. The ^{93}Nb MAS NMR spectra of PMN and PMN/PT compositions from 0.95PMN/0.05PT to 0.50PMN/0.50PT measured at 14.1 T are shown in Figure 6. With increased mol % $PbTiO_3$, there is a decrease in spectral resolution, and a decrease in the intensity of the sharp ^{93}Nb resonance near −902 ppm. A single broad symmetrical resonance at −1011 ppm is observed for high mol % PT systems, that is, 0.50PMN/0.50PT. The sharp ^{93}Nb NMR peak is not easily observed for 0.66PMN/0.34PT formed near the PMN/PT morphological phase boundary, and is nearly absent for the 0.50PMN/0.50PT sample. For the ^{93}Nb MAS spectra of the series of PMN/PT materials, the overall line shape of the broad resonance feature centered near −980 ppm for PMN is also observed to change substantially (see Figure 7), particularly for PMN/PTs at higher mol % PT. These ^{93}Nb NMR spectral changes observed for PMN/PT solid-solutions up to 50 mol % PT are interpreted as resulting from changes in the Nb(V) sites induced by significant Ti(IV) ion occupancy of B-sites in the PMN perovskite lattice. The 0.66PMN/0.34PT material formed at the MPB (see Figure 1),[16] in particular, also has accompanying changes in long-range order corresponding to a rhombohedral to tetragonal crystal lattice transition based on the PT composition and the powder XRD results as given in Figure 3.

Several significant changes are also readily apparent for the series of PMN/PT solid-solutions over the mol % PT range studied as shown by the two-dimensional ^{93}Nb nutation spectra (see Figure 6, B/B′−F/F′). First, for the ^{93}Nb nutation spectra of PMN/PT for lower mol % PT ($x = 0.05$ and 0.10, Figure 6, B and C), there is a significant reduction in the intensity or a broadening in F2 of the resonance with intermediate C_Q (∼17 MHz). Second, the intensity of the sharpest resonance at $1\nu_{rf}$ with the smallest C_Q < 0.8 MHz decreases for PMN/PTs at 0.90PMN/0.10PT and higher mol % PT at a 3.4 μs refocusing pulse length (Figure 6, C−F). Third, the line shape of the broadest resonance (C_Q > 62 MHz) significantly changes and the peak position shifts (to a small extent) to lower frequency in the nutation dimension with added PT (Figure 6, B−F); the small shifts reflect smaller C_Q values.

Table 2. Summary of ^{93}Nb Resonances for PMN from ^{93}Nb MAS NMR and ^{93}Nb Nutation Results

δ_{obs} (^{93}Nb) From MAS	-900 ppm Sharp	-954 to -980 ppm Broad	
C_Q (^{93}Nb) From Nutation	< 0.8 MHz	≈ 17 MHz	> 62 MHz
Nb(V) Site Symmetry	Cubic	Axial (Tetragonal)	Rhombic
Assignment of $Nb(ONb)_{6-x}(OMg)_x$ Configurations	$Nb(OMg)_6$	$Nb(ONb)_{6-x}(OMg)_x$ (x = 1 to 5)	

Discussion of ^{93}Nb MAS NMR and ^{93}Nb Nutation Results

Interpretation of ^{93}Nb MAS NMR and ^{93}Nb Nutation of PMN and PMN/PT. The solid-state ^{93}Nb MAS NMR spectra reported here have at least two distinctly different ^{93}Nb resonances for both PMN and PMN/PT solid-solution materials below its MPB composition of 34 mol % PT (Figure 1), while ^{93}Nb nutation spectra have three different resonances with a range of different C_Q values. A summary of the relationship between the assignments for the ^{93}Nb MAS NMR and ^{93}Nb nutation results is given in Table 2. The sharp ^{93}Nb MAS NMR resonance at ∼−902 ppm (Figure 4) is correlated with the ^{93}Nb nutation resonance with a small quadrupolar coupling constant (C_Q < 0.8 MHz); it has little residual second-order quadrupolar line-broadening consistent with this resonance corresponding

to Nb(V) ion B-sites approaching local cubic symmetry. This near-cubic symmetry is likely a consequence of the local Mg/Nb ordering. The intensity decreases with the substitution of Ti(IV) ions into the B-sites causing a reduction in the symmetry of some near-cubic Nb(V) sites. The ^{93}Nb NMR frequency shift of −902 ppm is substantially lower than the frequency shifts reported for distorted $Nb(ONb)_6$ configurations measured for alkali niobates (−1028 to −1102 ppm) and lead niobate pyrochlores (−975 to −1020 ppm) as summarized in Table 1.[73,74]

The broad ^{93}Nb MAS NMR resonance centered near −980 ppm for polycrystalline PMN and PMN/PT (Figure 7) up to the MPB (34 mol %) likely consists of two or more overlapping powder patterns with different residual second-order quadrupolar contributions to their line shapes not removed by MAS, corresponding to the two nutation ^{93}Nb resonances of intermediate and large quadrupolar coupling constants ($C_Q \approx 17$ MHz and > 62 MHz, respectively). The large line width is consistent with some of these Nb(V) sites having larger C_Q values than observed for alkali niobates (∼17 to 23 MHz).[55−58,73] The lower site symmetry (and corresponding large C_Q values) observed for this broad signal at −980 ppm is likely due to the effects of both neighboring B-cation distribution effects on the Nb(V) cations, that is, Mg/Ti/Nb disorder, that alters the local niobium−oxygen bond lengths and O−Nb−O bond angles, and the effects of nearest-neighbor A-site Pb(II) ions on the NbO_6 site bonding and symmetry. Line shape changes of the broad resonance near −980 ppm are not, however, apparent in the spectra obtained on lower mol % PT materials (Figure 7A−D).

For polycrystalline 0.66PMN/0.34PT, the most significant change in the ^{93}Nb MAS NMR spectra (Figure 7) is the virtual disappearance of the sharp signal near −902 ppm and the line shape changes in the −980 ppm resonance to a broad symmetrical peak near −1000 ppm. Related changes in contour plots and F1 projections (not shown) of the ^{93}Nb nutation spectra of PMN/PTs are also observed for compositions at the MPB, where long-range pseudo-rhombohedral to tetragonal crystal lattice structural changes for PMN/PT occurs. At the high mol % PT compositions, the loss in intensity of the ^{93}Nb signal at −902 ppm is also attributed to Ti(IV) ion incorporation into the majority of B-sites in PMN, thus reducing the Nb(V) ion B-site symmetry in the Mg-rich regions of PMN. The loss of the characteristic line shape features of the broad −980 ppm signal is also most apparent at 34 and 50 mol % PT due to increased disorder from significant B-site occupation by three different cations. The B-site disorder likely results in increased chemical shift dispersion and a range of quadrupolar coupling constants for the ^{93}Nb resonance near −980 ppm. The two broad ^{93}Nb nutation resonances with different quadrupolar coupling constants are consistent with two types of Nb(V) B-sites having different chemical environments due to different local Nb−O bond lengths and O−Nb−O bond angles. The differences in the local oxygen symmetry and/or distortions around the Nb(V) B-site ions are likely caused by different next-nearest neighbor B-site cations (Mg/Ti/Nb) configurations, and/or differences caused by different arrangements of the nearest-neighbor A-site Pb(II) cations. In addition, the different motional behavior associated with these two different Nb(V) B-sites, in the compositional PMN/PT range studied here, may also contribute to their complex ^{93}Nb MAS and ^{93}Nb nutation spectral behavior.

Local Mg/Nb B-Site Configurations and Ordering from ^{93}Nb NMR Spectra. On the basis of the 2:1 Nb/Mg stoichiometry for the B-sites in the PMN perovskite lattice structure, and recent HRTEM measurements and XRD calculations[4,18,19] supporting the presence of local Mg-rich and Nb-rich regions in PMN, the narrower, lower intensity, ^{93}Nb signal at −902 ppm (∼10%) is tentatively assigned to Nb(V) B-sites in Mg-rich regions, while the broader ^{93}Nb resonance centered at −980 ppm is tentatively assigned to two different types of Nb(V) ions in the B-sites of Nb-rich regions.

PMN materials with a perovskite lattice may be ideally described by an ordered distribution of Mg(II)/Nb(V) ions in the next-nearest neighbor (nnn) B-site octahedra as depicted in Figure 2. However, a large degree of disorder in the B-site Mg/Nb cation distribution exists, where numerous possible nnn B-site cation configurations may occur in PMN as shown in Figure 8A (top). For the 10 possible nnn Mg/Nb B-site configurations given in Figure 8B, recent EPR studies of single crystal and polycrystalline PMN,[43,44] and ^{93}Nb MAS NMR of single-crystal PMN and PZN[49] support the classification of the nnn B-site configurations into local cubic, axial (or tetragonal), and rhombic symmetries.

In Figure 8B, the nearest-neighbor oxygens that produce the largest effects on the local chemical environment of the Nb(V) ions have been omitted for clarity; the next-nearest neighbor A-site Pb(II) ions have also been omitted. While the local oxygen environments contribute the largest extent to the observed chemical shift and quadrupolar parameters for the ^{93}Nb resonances, different arrangements of the second nearest-neighbor Mg(II) or Nb(V) cations cause significant changes in both the Nb−O covalency and the Nb−O bond lengths and symmetry of the NbO_6 octahedra. The second nearest-neighbor B-site cations are likely the origin of the significant perturbations of the local oxygen chemical environments around the Nb(V) B-sites observed by ^{93}Nb NMR. As shown in A (top) and B of Figure 8, the local Mg/Nb octahedra B-site arrangements in PMN may be disordered in contrast to the repeating MgNbNb order (Figure 2), causing a wide distribution of different Nb(V) site configurations corresponding to a range of **Nb**-$(ONb)_{6-x}(OMg)_x$ nearest-neighbor B-site cations, where $x = 0$, 1, 2, ..., 6. Whether a random degree of disorder or partial Mg/Nb ordering exists is not clear due to the broad distribution of resonances in the ^{93}Nb MAS NMR spectra (−900 to −1200 ppm). The interpretation of the ^{93}Nb NMR results for PMN and PMN/PT materials at low mol % PT, however, are consistent with a partially disordered Mg/Nb B-site structural model as proposed from HRTEM studies[17−20,28−34] based on the two ^{93}Nb resonances assigned to Nb(V) B-sites in Mg(II)-rich and a Nb(V)-rich nanodomain regions. The latter Nb-rich regions must due to the chemical stoichiometry of PMN have magnesium next-nearest neighbor B-site ions in the axial and rhombic configurations (Figure 8B).

The interpretation of the frequency shifts observed for the sharp −902 ppm resonance and the broad resonance centered at −980 ppm for PMN and related PT solid-solutions is not straightforward due to the absence of extensive literature information regarding the effects of local chemical environments on the ^{93}Nb frequency or chemical shifts. From the ^{93}Nb frequency shift and isotropic chemical shift results summarized in Table 1, it is apparent that the −902 ppm signal is unusual for B-site $Nb(ONb)_6$ configurations such as found for the three alkali niobate perovskites where the frequency shifts vary from −1028 to −1102 ppm (Table 1).[49,73] Recent extensive static and ^{93}Nb MAS NMR studies of the alkali niobates[73] reported elsewhere show $\delta_{iso}(^{93}Nb)$ values from −1000 to −1070 ppm. These distorted pseudo-octahedral B-site $Nb(ONb)_6$ configura-

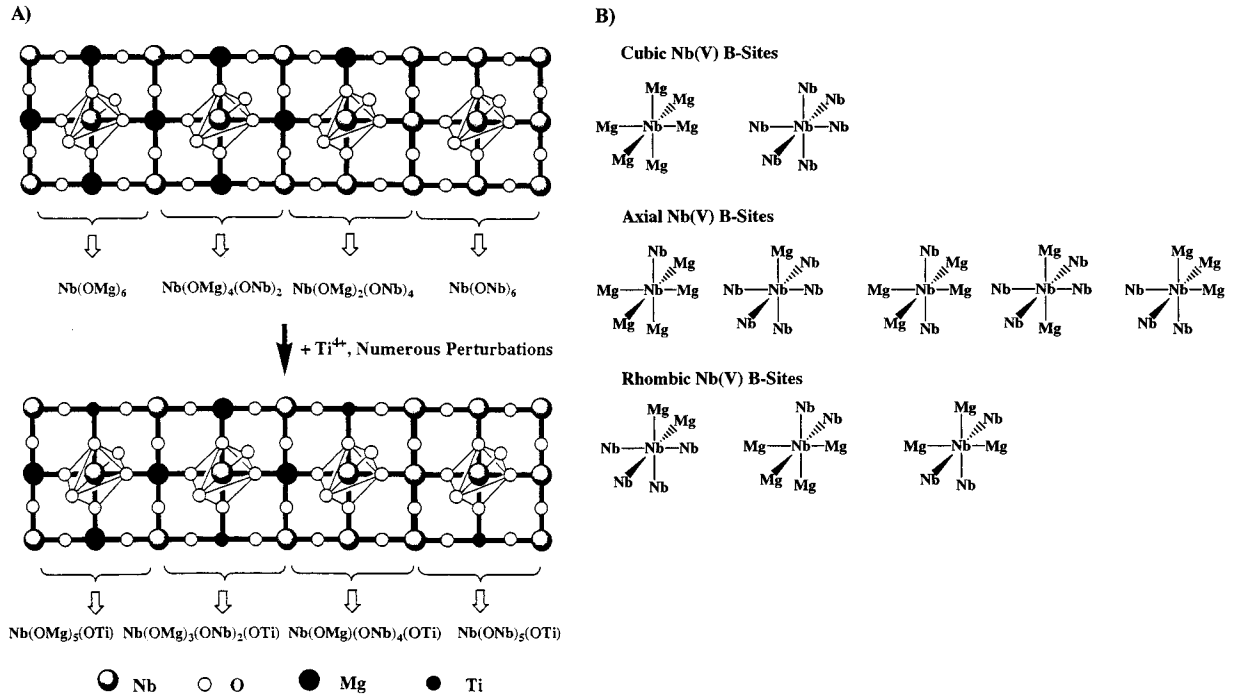

Figure 8. (A) Top: depiction of four possible arrangements of adjacent $Nb(OX)_6$ pseudo-octahedra, where X = Mg or Nb for PMN. The **Nb** octahedra are depicted for various arrangements of next-nearest neighbor cation configurations that exist due to disorder of the Mg/Nb cations causing a distribution of Nb(V) sites of $Nb(ONb)_{6-x}(OMg)_x$ nearest-neighbor B-site configurations, where $x = 0-6$. Bottom: depiction of four possible arrangements of adjacent $Nb(OX)_6$ pseudo-octahedra, where X = Mg or Nb or Ti for PMN/PT. The **Nb** centers are depicted by four octahedra. Possible arrangements of next-nearest neighbor cation configurations exist due to disorder of the Mg/Nb/Ti cations causing a distribution of Nb(V) ion sites of $Nb(ONb)_{6-(x+y)}(OMg)_x(OTi)_y$ nearest-neighbor B-site configurations, where x and $y = 0-6$. (B) Depiction of 10 possible arrangements of cubic, axial and rhombic Nb(V) sites with nearest neighbor B-site MgO_6 or NbO_6 configurations for PMN.

tions have large C_Q values from 17 to 23 MHz that may be contrasted with the low C_Q for the −902 ppm signal in PMN. Comparison of the frequency shifts and small C_Q values for the −902 ppm resonance for PMN and low-PT content PMN/PTs suggest that this signal is associated with 1:1 Mg/Nb ordering in Mg-rich regions where the local symmetry is near-cubic, i.e., $Nb(OMg)_6$ configurations, in contrast to the $Nb(ONb)_{6-x}(OMg)_x$ configurations in the Nb-rich regions of PMN that are assigned to the broad ^{93}Nb resonance near −980 ppm and the distorted $Nb(ONb)_6$ configurations in the alkali niobates that are observed from −1028 to −1102 ppm. It should also be noted that the quadrupolar induced frequency shift for the $Nb(ONb)_6$ site in $PbNb_2O_6$ is ∼ −19 ppm (−1134 ppm compared to δ_{iso} equal −1115 ppm, see Table 1) for the single ^{93}Nb resonance for $PbNb_2O_6$. Thus, quadrupolar frequency shifts on the order of ∼ −19 to −32 ppm are in the range observed for alkali niobates of the perovskite structure and the low-temperature form of lead metaniobate of a nonperovskite lattice, that all have $Nb(ONb)_6$ B-site configurations with moderate C_Q (16 to 23 MHz) values.[50,73,74]

For the broad ^{93}Nb NMR resonance centered at −980 to −1000 ppm for PMN and related PMN/PTs up to 34 mol % PT, this frequency shift region is comparable to that observed for corner-shared pseudo-octahedral $Nb(ONb)_6$ sites of varying degrees of distortion found in lead niobates (Table 1).[74] The frequency shifts for the lead niobates span −975 ppm to −1020 ppm, except for lead metaniobate (δ_{obs} = −1134 ppm; δ_{iso} = −1115 ppm), compared to the −1028 to −1102 ppm (δ_{iso} = −1000 to −1070) range observed for the alkali niobates. The frequency shift range −975 to −1020 ppm and the C_Q values (12 to 21 MHz) observed for the lead niobates pyrochlores, $Pb_2Nb_2O_7$, $Pb_3Nb_4O_{13}$ (cubic), $Pb_3Nb_2O_8$, and $Pb_5Nb_4O_{15}$, are consistent with distorted corner-shared $Nb(ONb)_6$ sites.[74] PMN pyrochlore ($Pb_{1.83}Nb_{1.71}Mg_{0.29}O_{6.39}$) is also observed to have a frequency shift in this range (−1012 ppm) but may be contrasted with the lead niobate pyrochlores, since it contains a 6:1 Nb/Mg mole ratio, that is considerably lower in magnesium content than PMN. Based on these similarities, the broad −980 ppm resonance in PMN and PMN/PT is assigned to a range of axial or rhombic $Nb(ONb)_{6-x}(OMg)_x$ B-site configurations as depicted in Figure 8B, for $x = 0-5$. These Nb(V) B-site configurations occur in Nb-rich regions of PMN and PMN/PT, with partial Mg/Nb B-site disorder and varying Mg/Nb compositions, and depend on spatial relationships to various next-nearest neighbor Mg/Nb cations.

The interpretation of the ^{93}Nb MAS NMR and ^{93}Nb nutation studies reported here is consistent with recent EPR studies of single-crystal and polycrystalline PMN,[43,44] ^{93}Nb MAS NMR studies of single-crystal PMN and PZN,[49] and high-resolution TEM studies of PMN.[18] The EPR studies have provided indirect evidence for the presence of cubic, axial, and rhombic B-sites in PMN by measurement of the symmetry-related EPR parameters of Fe(III) ion-doped in PMN.[43,44] Recent ^{93}Nb MAS NMR spectra of single-crystal PMN and PZN[49] indicate that at least two resonances attributed to local regions with different Mg/Nb configurations exist in these materials. In addition, HRTEM studies to 0.2 nm resolution of the nanodomain textures and structures in PMN have revealed considerable details regarding such local domain regions containing ordered and disordered Mg/Nb B-sites.[18] The HRTEM images and related simulations, together with crystal lattice energy calculations, predict the relative stability of various domain regions with both ordered and disordered distributions of Mg/Nb B-sites. Using a model involving next-nearest neighbor B-site configurations, several local Mg/Nb configurations or structural clusters of such configurations were postulated for the two different types of B-site nanodomains in the three-dimensional structure of PMN based on their substructural stoichiometry:[4,17−20,28−34]

$$\text{“}Pb_3MgNb_2O_9\text{”} \rightarrow \underset{\text{(PMN)}}{}$$

$$[Pb_2MgNbO_6]^- + [PbNbO_3]^+$$

Mg(II)-Rich Negative Regions — Nb(V)-Rich Positive Regions

The so-called “1:1 ordered” regions have Mg and Nb ions arrayed in a successive order (Mg−O−Nb local order) with a 1:1 Mg/Nb mole ratio. Such “Mg(II)-rich” regions of the composition $[Pb_2MgNbO_6]^-$ would be negatively charged and nonstoichiometric, and are compensated by surrounding positively charged “Nb(V)-rich” regions (with increased local Nb−O−Nb ordering) of composition $[PbNbO_6]^+$ required to maintain the charge neutrality.[18,33,34] From HRTEM studies, seven different types of defect clusters, where the local Mg/Nb stoichiometry deviate from the 2:1 Nb/Mg ratios, were proposed, including two local configurations for the Mg(II)-rich regions: **Nb**$(OMg)_6$ or **Mg**$(OMg)_6$ with cubic symmetry, and **Nb**$(ONb)_2(OMg)_4$ or **Nb**$(ONb)_3(OMg)_3$ configurations with axial symmetry; and three local configurations in the Nb-rich regions: **Nb**$(ONb)_6$ with cubic symmetry, **Nb**$(ONb)_5(OMg)$ with axial symmetry, and **Nb**$(ONb)_4(OMg)_2$ or **Nb**$(ONb)_3(OMg)_3$ with rhombic symmetry.[18]

The types of next-nearest neighbor Nb(V) B-site configurations shown in Figure 8B, therefore, can account for the different local Nb(V) sites of different symmetries due to various Mg/Nb cation ordering, consistent with the ^{93}Nb MAS NMR and nutation results. As shown in Figure 8A, these different types of sites may be arranged proximal to each other in a complex three-dimensional structural organization in PMN. While the resonances with minimal ($<$0.8 MHz) or moderate ($\sim$17 MHz) quadrupolar coupling constants may be due to local cubic (one possible) or axial (three possible) Mg/Nb second nearest neighbor B-site configurations, respectively, the broadest resonance is likely due to a range of highly distorted local NbO_6 octahedra of rhombic symmetry (five or more possible). The nnn B-site cations significantly influence the local oxygen environments, that is, Nb−O bond lengths and/or O−Nb−O angles, for different nnn $Nb(OX)_6$ octahedra due to cation size differences ($r_{Mg^{2+}} = 0.72$ Å vs $r_{Nb^{5+}} = 0.64$ Å).

The high-temperature reaction of PMN and PT mixtures to form PMN/PT solid-solutions results in incorporation of Ti(IV) ions in the B-sites of PMN. The ^{93}Nb MAS NMR and ^{93}Nb nutation spectra of PMN/PT materials are substantially different than those of PMN. The incorporation of Ti(IV) into the B-sites may occur by a large number of B-site perturbations, as depicted in Figure 8A (bottom), thus leading to decreased Nb(V) B-site symmetry for most of the sites as a result of disorder of these three different cations. Assuming that PT dissolution into various regions of solid PMN is nonselective, this B-site disorder should also increase the chemical shift dispersion contribution to the broad ^{93}Nb resonance (−980 ppm) due to a larger range of different Nb(V) sites, particularly at high mol % PT ($>$25 mol %).

Conclusions

The ^{93}Nb MAS NMR and ^{93}Nb nutation studies described demonstrate the significant capabilities of these spectroscopic approaches to obtain new atomic-level information about the local Nb(V) B-site environments in piezoelectric PMN and PMN/PT systems. The ^{93}Nb nutation spectra have three different ^{93}Nb resonances assigned to local Nb(V) sites with different symmetries based on both chemical shift and quadrupolar parameters. The three types of Nb(V) B-sites in PMN are interpreted as due to different local Nb−O environments as a result of different B-site (Mg/Nb) configurations. The ^{93}Nb MAS NMR and nutation spectral features are assigned to a range of different B-site Mg/Nb configurations with local cubic, axial and rhombic symmetry, thus accounting for the quadrupolar coupling constants ($<$0.8, $\sim$17, and $>$62 MHz) estimated for these types of Nb(V) sites. PMN likely consists of partially ordered Mg/Nb B-site occupancy with high symmetry near-cubic Nb(V) sites (sharp ^{93}Nb signal at −902 ppm) associated with nnn $Nb(OMg)_6$ configurations in Mg(II)-rich ordered domain regions. The two broader ^{93}Nb NMR resonances with intermediate and high C_Q values are assigned to two types of lower symmetry B-site NbO_6 octahedra with local nnn $Nb(ONb)_{6-x}(OMg)_x$ (where $x = 0$ to 5) configurations. One set of configurations has local axial symmetry, and another has lower rhombic symmetry. Thus, polycrystalline PMN has a range of three distinct types of distorted NbO_6 octahedra, with the atomic-level Mg/Nb disorder causing the local Nb(V) B-site regions to exhibit different microscopic dipolar behavior. These different local B-site Nb(V) (and also Mg(II)) dipoles are postulated to be the origin of the diffuse nature of the macroscopic crystal lattice phase transitions observed for PMN.

The ^{93}Nb MAS NMR and ^{93}Nb nutation studies of PMN/PT solid-solutions have also provided unique, but less specific, atomic-level information about the Nb(V) B-sites in these complex solid-solution ferroelectric materials. Low mol % PT additions result in changes in both the ^{93}Nb MAS NMR and nutation spectra consistent with substitution of Ti(IV) ion for both Mg(II) and Nb(V) in the B-sites of PMN. The increased chemical B-site disorder due to three B-site cations (Mg/Ti/Nb) causes the near disappearance of the sharp ^{93}Nb signal due to near-cubic $Nb(OMg)_6$ site configurations at the MPB, and the line shape changes for the two broader ^{93}Nb resonances assigned to axial and rhombic $Nb(ONb)_{6-x}(OMg)_x$ site configurations in the Nb(V)-rich regions of PMN at $>$10 mol % PT. The Ti(IV) substitution for Nb(V) in both the Mg(II)-rich and Nb(V)-rich regions of PMN is postulated to be nonselective.

These investigations have significantly clarified our understanding of the Mg/Nb and Mg/Ti/Nb B-site chemical disorder in PMN and PMN/PT systems, as well as provided a more detailed description of the local NbO_6 site symmetries associated with the range of Nb(V) B-sites found in these materials. Experimental support for distinctly different Nb(V) B-sites located in Mg(II)- and Nb(V)-rich nanodomain regions in PMN and PMN/PT materials at low PT contents is also presented. Further detailed variable temperature ^{93}Nb MAS NMR and ^{93}Nb nutation studies of PMN and PMN/PTs above and below the diffuse phase transitions temperatures are in progress to address the temperature-dependent ^{93}Nb NMR relaxation behavior and the Nb(V) B-site motion in these materials. Such investigations may also elucidate the relative motional differences of specific Nb(V) B-site NbO_6 octahedra of different Mg/Ti/Nb configurations that likely occur in the Mg(II)-rich and Nb(V)-rich regions of these important ferroelectric materials.

Acknowledgment. This work was supported by a Department of Defense University Research Initiative Support Program (URISP) grant administered by the Office of Naval Research, Grant 0014-96-1-0781. The authors acknowledge Dr. Peidong Zhao for contributions to developments in 2D ^{93}Nb nutation experiments, and Professor Gary E. Maciel and Dr. Herman Lock, Colorado State University NMR Center, for use of the Chemagnetics CMX-600 spectrometer.

JA990688J